LAWRENCE
LIVERMORE
NATIONAL
LABORATORY

LLNL-JRNL-409903

High Order Well-Balanced Schemes and Applications to Non-Equilibrium Flow with Stiff Source Terms

W. Wang, C.-W. Shu, H. C. Yee, B. Sjogreen

January 15, 2009

Journal of Computational Physics

Disclaimer

High Order Well-Balanced Schemes and Applications to Non-Equilibrium Flow with Stiff Source Terms

Wei Wang*, Chi-Wang Shu†, Helen C. Yee‡and Bjorn Sjögreen§

January 13, 2009

Abstract

The stiffness of the source terms in modeling non-equilibrium flow problems containing finite-rate chemistry or combustion poses additional numerical difficulties beyond that for solving non-reacting flows. A well-balanced scheme, which can preserve certain non-trivial steady state solutions exactly, may help to resolve some of these difficulties. In this paper, a simple one dimensional non-equilibrium model with one temperature is considered. We first describe a general strategy to design high order well-balanced finite difference schemes and then study the well-balanced properties of high order finite difference weighted essentially non-oscillatory (WENO) scheme, modified balanced WENO schemes and various TVD schemes. The advantages of using a well-balanced scheme in preserving steady states and in resolving small perturbations of such states will be shown. Additional numerical examples are provided to verify the good resolution, in addition to the well-balancedness, for both smooth and discontinuous solutions as well.

Key words: Well-balanced schemes, non-equilibrium flow, stiff source terms, chemical reactions, WENO schemes, TVD schemes, nozzle flow.

1 Introduction

In the modeling of unsteady reactive problems, the interaction of turbulence with finite-rate chemistry introduces a wide range of space and time scales, leading to additional numerical difficulties. A main difficulty stems from the fact that most numerical algorithms used in reacting flows were originally designed to solve non-reacting fluids. As a result, spatial stiffness due to the reacting source terms and turbulence/chemistry interaction are major stumbling blocks to numerical algorithm development. One of the important numerical issues is the proper numerical treatment of a system of highly coupled stiff non-linear source terms, which will result in possible spurious steady state numerical solutions (see Lafon and Yee [14, 15]). It was also shown in Lafon and Yee [14, 15] that various ways of discretizing the reaction term can affect the stability of, and convergence to, the spurious numerical steady states and/or the exact steady states. Pointwise evaluation of the source terms appears to be the least stable (see [14, 15, 6, 2]).

*Center for Turbulence Research, Stanford University, Stanford, CA 94305
†Division of Applied Mathematics, Brown University, Providence, RI 02912
‡NASA Ames Research Center, Moffett Field, CA 94035
§Lawrence Livermore National Laboratory, Livermore, CA 94551.

A well-balanced scheme (for time-dependent PDEs), as coined by LeVeque [16], which can preserve certain nontrivial steady state solutions exactly, may help to solve this spurious numerical behavior. Most work about well-balanced schemes developed in the literature is for the shallow water equations (e.g. [5, 8, 9, 11, 13, 19, 21, 26, 33]). We follow the work by Xing and Shu in 2005 [24]. They develop a well-balanced high order finite difference weighted essentially non-oscillatory (WENO) scheme for solving the shallow water equation, which is non-oscillatory, well-balanced for still water, and genuinely high order in smooth regions. In [25], they generalize the high order well-balanced WENO scheme to solve a wider class of hyperbolic systems with separable source terms. In our paper, we apply their approach and construct high order well-balanced WENO scheme to the non-equilibrium flow with reaction terms.

The procedure only for the one dimensional case is described in this paper. Generalizations to multi-dimensions can be done for some cases, following the same procedure as in [24]. The one-dimensional hyperbolic system of conservation laws with source terms under consideration is:

$$U_t + F(U, x)_x = S(U, x), \tag{1}$$

where U is the solution vector, $F(U, x)$ is the flux and $S(U, x)$ is the source term. This balance law admits steady state solutions in which the source term is exactly balanced by the flux gradient. The objective of well-balanced schemes is to preserve exactly some of these steady state solutions. In the non-equilibrium flow containing finite-rate chemistry, the source term represents the production of species from chemical reactions. One important property of the source term for non-equilibrium flow (which may make the work easier) is that it does not depend on the spatial grid x, i.e. $S(U, x) \equiv S(U)$. Thus, there is no need to consider the spatial discretization for the source term. Furthermore, the source term even does not depend on the dimensions.

The well-balanced property of various popular linear and non-linear numerical schemes in the literature is studied based on a simple one dimensional model with one temperature and three species (O_2, O and N_2). This model is obtained by reducing the model by Gnoffo, Gupta & Shinn [4]. The different behaviors of those numerical schemes in preserving steady states and in resolving small perturbations of such states will be shown. The high order balanced WENO schemes are also designed and then applied for the problems.

We will show that for the stationary steady state solutions of the reactive flow, the well-balanced schemes will give machine round-off errors regardless of the mesh sizes, while the non-well balanced schemes give truncation errors consistent with the formal order of accuracy for the schemes. For a small perturbation of such steady state solutions, the well-balanced schemes can resolve them well with very coarse meshes, while the non-well balanced schemes would give spurious structures in the numerical solutions, which will decrease and eventually disappear with a mesh refinement. Our work indicates the advantage of well-balanced schemes: they can be used to resolve small perturbations of the steady state solutions using much coarser meshes than that for the non-well balanced schemes, thereby saving a lot of CPU time, especially with the number of species increased.

Numerical tests also includes high-temperature shock tube and nozzle flows. It will show that the well-balanced schemes will not lose any accuracy or other good properties such as shock capturing for approximating solutions away from the steady state. We remark that although our numerical simulations are performed only for the three species model, the procedure of designing well-balanced schemes is general for any number of species.

2 Governing equations

Assuming no conduction or radiation, the considered non-equilibrium models are a system of hyperbolic conservation laws with source terms, denoted by

$$U_t + F(U)_x = S(U). \tag{2}$$

Here U, $F(U)$ and $S(U)$ are column vectors with $m = n_s + 2$ components where n_s is the number of species.

$$U = (\rho_1, \ldots, \rho_{n_s}, \rho v, \rho e_0)^T, \tag{3}$$

$$F(U) = (\rho_1 v, \ldots, \rho_{n_s} v, \rho v^2 + p, \rho v e_0 + vp)^T, \tag{4}$$

$$S(U) = (s^1, \ldots, s^{n_s}, 0, 0)^T, \tag{5}$$

where ρ_s is the density of species s. The total density is defined as $\rho = \sum_{s=1}^{n_s} \rho_s$ and the pressure p is given by

$$p = RT \sum_{s=1}^{n_s} \frac{\rho_s}{M_s}, \tag{6}$$

where M_s is the molar mass of species s. The temperature T can be found from the total energy

$$\rho e_0 = \sum_{s=1}^{n_s} \rho_s e_{i,s}(T) + \sum_{s=1}^{n_s} \rho_s h_s^0 + \frac{1}{2}\rho v^2, \tag{7}$$

where $e_{i,s} = C_{v,s}T$ is the internal energy with $C_{v,s} = 3R/2M_s$ and $5R/2M_s$ for monoatomic species and diatomic species, respectively, and the enthalpies h_s^0 are constants.

The source term $S(U)$ describes the chemical reactions occurring in gas flows which result in changes in the amount of mass of each chemical species. We assume there are J reactions of the form

$$\nu'_{1,j} X_1 + \nu'_{2,j} X_2 + \cdots + \nu'_{n_s,j} X_{n_s} \rightleftharpoons \nu''_{1,j} X_1 + \nu''_{2,j} X_2 + \cdots + \nu_{n_s,j} X_{n_s}, \quad j = 1, \ldots, J, \tag{8}$$

where $\nu'_{1,j}$ and $\nu''_{1,j}$ are respectively the stoichiometric coefficients of the reactants and products of species i in the jth reaction. For non-equilibrium chemistry, the rate of production of species i due to chemical reaction, may be written as

$$s^i = M_i \sum_{j=1}^{J} (\nu''_{i,j} - \nu'_{i,j}) \left[k_{f,j} \prod_{s=1}^{n_s} \left(\frac{\rho_s}{M_s} \right)^{\nu'_{s,j}} - k_{b,j} \prod_{s=1}^{n_s} \left(\frac{\rho_s}{M_s} \right)^{\nu''_{s,j}} \right], \quad i = 1, \ldots, n_s. \tag{9}$$

For each reaction j, the forward and backward reaction rates, $k_{f,j}$ and $k_{b,j}$ are assumed to be known functions of temperature.

Let the Jacobian matrix $A = \partial F / \partial U$ with $(a^1, \ldots, a^m)$ being the eigenvalues of A,

$$(a^1, \ldots, a^m) = (v, \ldots, v, v + a, v - a), \tag{10}$$

where a is the so-called "frozen speed of sound". Denote R as the matrix whose columns are eigenvectors of A. Let $a^l_{j+1/2}, R_{j+1/2}$ denote the quantities a^l and R evaluated at some symmetric average of U_j and U_{j+1}, such as Roe's average [20]. Define

$$\alpha_{j+1/2} = R^{-1}_{j+1/2}(U_{j+1} - U_j) \tag{11}$$

as the difference of the local characteristic variables in the x direction.

In this paper, the considered schemes are the fifth-order finite difference WENO schemes [10, 22], second-order semi-implicit predictor-corrector TVD (P-C TVD) [30, 17], second-order symmetric [27] and Harten and Yee TVD scheme [29, 28] and second-order MUSCL scheme [28]. Except for the P-C TVD, the explicit TVD high order Runge-Kutta method [23] as well as the pointwise implicit additive Runge-Kutta (ARK) method [12] are used for time discretization (see Appendix A for more details).

3 Well-balanced WENO schemes and linear schemes

A well-balanced scheme refers to a scheme that preserves exactly specific steady state solutions of the governing equations.

We will first consider the 1-D scalar balance law

$$u_t + f(u,x)_x = g(u,x), \tag{12}$$

i.e., the steady state solution u satisfying

$$f(u,x)_x = g(u,x). \tag{13}$$

A linear finite difference operator D is defined to be one satisfying $D(af_1+bf_2) = aD(f_1)+bD(f_2)$ for constants a, b and arbitrary grid functions f_1 and f_2. A scheme for Eq. (12) is said to be a linear scheme if all the spatial derivatives are approximated by linear finite difference operators.

Xing & Shu [25] proved that under the following two assumptions regarding Eq. (12) and the steady state solution of Eq. (13), linear schemes with certain restrictions are well-balanced schemes. Furthermore, high-order non-linear WENO schemes can be adapted to become well-balanced schemes.

Assumption 1. *The considered steady state preserving solution u of Eq.* (13) *satisfies*

$$r(u,x) = \textit{constant}, \tag{14}$$

for a known function $r(u,x)$.

Assumption 2. *The source term g(u,x) can be decomposed as*

$$g(u,x) = \sum_i s_i(r(u,x))t_i'(x) \tag{15}$$

for a finite number of functions s_i and t_i.

A linear scheme applied to Eq. (13) would have a truncation error

$$D(f(u,x)) - \sum_i s_i(r(u,x))D_i(t_i(x)), \tag{16}$$

where D and D_i are linear finite-difference operators used to approximate the spatial derivatives. One restriction to the linear schemes is needed:

$$D_i = D \quad \text{for all } i \tag{17}$$

when applied to the steady state solution. For such linear schemes we have

Proposition 1. *For the balance law Eq.* (12) *with source term Eq.* (15)*, linear schemes with restrictions Eq.* (17) *for the steady state solutions satisfying* (14) *are well-balanced schemes.*

Proof. For the steady state solutions satisfying Eq. (14), the truncation error for such linear schemes with Eq. (17) reduces to

$$\begin{aligned} & D(f(u,x)) - \sum_i s_i(r(u,x)) D(t_i(x)) \\ = \; & D\left(f(u,x) - \sum_i s_i(r(u,x)) t_i(x) \right), \end{aligned}$$

where the linearity of D and the fact that $r(u,x)$ is constant for the steady state solution u are used. Note that for such steady state solution u, $f(u,x) - \sum_i s_i(r(u,x))t_i(x)$ is a constant, because

$$\begin{aligned} & \frac{d}{dx}\left(f(u,x) - \sum_i s_i(r(u,x)) t_i(x) \right) \\ = \; & f(u,x)_x - \sum_i s_i(r(u,x)) t_i'(x) \\ = \; & f(u,x)_x - g(u,x) = 0. \end{aligned}$$

Thus, the truncation error is zero for any consistent finite-difference operator D. Therefore, linear schemes with Eq. (17) preserve these steady state solutions exactly. □

Now the high-order non-linear finite-difference WENO schemes are considered in which the non-linearity comes from the non-linear weights and the smooth indicators. We follow the procedures described in Xing & Shu [24, 25] for the shallow water equations. First, for the situation without flux splitting (19) (e.g., the WENO-Roe scheme in [10]), the WENO approximation to f_x can be written as

$$f_x|_{x=x_j} \approx \sum_{k=-r}^{r} c_k f_{k+j} = D_f(f)_j,$$

where $r = 3$ for the fifth-order WENO approximation and the coefficients c_k depend non-linearly on the smoothness indicators involving the grid function $f_{j-r}, \ldots, f_{j+r}$. The key idea now is to use the finite difference operator D_f, and apply it to approximate $t_i'(x)$ in the source terms, i.e.,

$$t_i'(x_j) \approx \sum_{k=-r}^{r} c_k t_i(x_{k+j}) = D_f(t_i(x))_j. \tag{18}$$

Clearly, the finite-difference operator D_f, obtained from the high-order WENO procedure is a high-order linear approximation to the first derivative for any grid function. Therefore, the proof for Proposition 1 will be satisfied and we conclude that the high-order finite difference WENO scheme as stated above, without the flux splitting, and with the special handling of the source terms described above, maintains exactly the steady state.

Next, WENO schemes with a Lax-Friedrichs flux splitting , such as WENO-LF and WENO-LLF, are considered. The flux $f(u,x)$ is written as a sum of $f^+(u,x)$ and $f^-(u,x)$, defined by

$$f^{\pm}(u) = \frac{1}{2}(f(u) \pm \alpha u), \tag{19}$$

where α is taken as $\alpha = \max_u |f'(u)|$ (see [10, 22] for more details). In order to obtain a well-balanced scheme, the $\pm\alpha u$ in the Lax-Friedrichs flux splitting (19) is replaced with

$$\pm\alpha \text{sign}\left(\frac{\partial r(u,x)}{\partial u}\right) r(u,x), \tag{20}$$

where we would need to assume that $\frac{\partial r(u,x)}{\partial u}$ does not change sign. The constant α should be suitably adjusted by the size of $\frac{\partial r(u,x)}{\partial u}$ in order to maintain enough artificial viscosity (see [25] for more details).

The framework described for the scalar case can be easily applied to systems (1). For a system with m equations, we would have m relationships in the form of Eq. (14):

$$r_l(U,x) = \text{constant}, \quad l = 1, \ldots, m. \tag{21}$$

In Assumption 2, s_i could be arbitrary functions of $r_l(U,x)$, and s_i and t_i can be different for different components of the source vector. The characteristic decomposition procedure does not alter the argument presented for the scalar case (see [24]). The modified WENO schemes through the procedure above will maintain exactly the steady state and will be called "balanced WENO" schemes in the paper.

However, the modification of the viscosity coefficient α in the Lax-Friedrichs building block in order to obtain well-balancedness for the steady state may adversely affect stability near strong shocks for solutions far away from the steady state, if Eq. (20) is used to obtain the well-balanced WENO-LF scheme for the system case. Here an equilibrium limiter is introduced, similar to the one used in [18], to determine whether the region is near the steady state or far away from the steady state. The Lax-Friedrichs flux splitting (19) is changed to

$$f^{\pm}(u) = \frac{1}{2}(f(u) \pm \alpha\lambda u), \tag{22}$$

with

$$\begin{aligned} \lambda := \quad & \max\left(\min\left(1, \frac{(|r_1(U_{i+1},x_{i+1})-r_1(U_i,x_i)|+|r_1(U_{i-1},x_{i-1})-r_1(U_i,x_i)|)^2}{|r_1(U_{i+1},x_{i+1})-r_1(U_i,x_i)|^2+|r_1(U_{i-1},x_{i-1})-r_1(U_i,x_i)|^2+\varepsilon}\right), \ldots, \right. \\ & \left. \min\left(1, \frac{(|r_m(U_{i+1},x_{i+1})-r_m(U_i,x_i)|+|r_m(U_{i-1},x_{i-1})-r_m(U_i,x_i)|)^2}{|r_m(U_{i+1},x_{i+1})-r_m(U_i,x_i)|^2+|r_m(U_{i-1},x_{i-1})-r_m(U_i,x_i)|^2+\varepsilon}\right)\right), \end{aligned} \tag{23}$$

where ε is a small number to avoid zero in the denominator and we take it as 10^{-6} in the computation. λ returns one in the smooth region if the solution is far from the steady state and then the scheme is the regular WENO-LF scheme. This guarantees that the limiter does not affect the high order accuracy of the scheme in smooth region for general solutions of Eq. (2). In the steady state, since all the r_l $(l = 1, \ldots, m)$ are constants, λ returns zero and then the scheme maintains the exact solutions for the steady state. To avoid confusion with "balanced WENO" schemes mentioned above, the WENO-LF with flux splitting (22) and equilibrium limiter (23) will be called "hybrid WENO-LF".

Finally, the well-balanced properties of various TVD schemes mentioned in Sec. 2 will be investigated. The semi-implicit Predictor-Corrector TVD scheme [30, 17] for Eq. (2) has the form

$$\left[1 - \frac{1}{2}\Delta t S'(U_j^n)\right] \Delta U_j^{(1)} = -\frac{\Delta t}{\Delta x}\left(F_j^n - F_{j-1}^n\right) + \Delta t S_j^n \tag{24}$$

$$U_j^{(1)} = \Delta U_j^{(1)} + U_j^n \tag{25}$$

$$\left[1 - \frac{1}{2}\Delta t S'(U_j^n)\right] \Delta U_j^{(2)} = -\frac{\Delta t}{\Delta x}\left(F_{j+1}^{(1)} - F_j^{(1)}\right) + \Delta t S_j^n \tag{26}$$

$$U_j^{(2)} = \Delta U_j^{(2)} + U_j^{(1)} \tag{27}$$

$$U_j^{n+1} = U_j^n + \frac{1}{2}\left(\Delta U_j^{(1)} + \Delta U_j^{(2)}\right) + \left[R_{j+1/2}^{(2)}\Phi_{j+1/2}^{(2)} - R_{j-1/2}^{(2)}\Phi_{j-1/2}^{(2)}\right]. \tag{28}$$

The third step Eq. (28) acts as a non-linear filter step [31]. The elements of the vector $\Phi_{j+1/2}$, denoted by $\phi_{j+1/2}^l$ with $l = 1, \ldots m$ are

$$\phi_{j+1/2}^l = \frac{1}{2}\left[\psi(\nu_{j+1/2}^l) - (\nu_{j+1/2}^l)^2\right]\left(\alpha_{j+1/2}^l - \hat{Q}_{j+1/2}^l\right), \tag{29}$$

where

$$\nu_{j+1/2}^l = \frac{\Delta t}{\Delta x} a_{j+1/2}^l. \tag{30}$$

The function $\psi(z)$ is an entropy correction to $|z|$. One possible form is in [28]

$$\psi(z) = \begin{cases} |z| & |z| \geq \delta_1 \\ (z^2 + \delta_1^2)/2\delta_1 & |z| < \delta_1 \end{cases}, \tag{31}$$

where δ_1 is the entropy fix parameter. See [32] for a discussion. $\hat{Q}_{j+1/2}^l$ is an unbiased limiter function which can be

$$\hat{Q}_{j+1/2}^l = \text{minmod}(\alpha_{j-1/2}^l, \alpha_{j+1/2}^l) + \text{minmod}(\alpha_{j+1/2}^l, \alpha_{j+3/2}^l) - \alpha_{j+1/2}^l \tag{32}$$

with

$$\text{minmod}(a, b) = \text{sgn}(a) \cdot \max\{0, \min[|a|, b\,\text{sgn}(a)]\}. \tag{33}$$

In this study, only diffusive limiters are considered. If a "smooth" limiter is preferred, then the minmod function $\text{minmod}(a, b)$ is replaced by the following smooth function

$$g(a, b) = [a(b^2 + \delta_2) + b(a^2 + \delta_2)]/(a^2 + b^2 + 2\delta_2), \tag{34}$$

where δ_2 is a small parameter between 10^{-7} to 10^{-5}. The predictor step Eq. (24) and the corrector step Eq. (26) are linear. However, the last filter step is not linear. We will explore this further in the next section.

The numerical flux $\hat{F}_{j+1/2}$ for the second-order symmetric TVD scheme [27] is described as

$$\hat{F}_{j+1/2} = \frac{1}{2}(F_j + F_{j+1} + R_{j+1/2}\Phi_{j+1/2}), \tag{35}$$

where

$$\phi_{j+1/2}^l = -\psi(a_{j+1/2}^l)(\alpha_{j+1/2}^l - \hat{Q}_{j+1/2}^l). \tag{36}$$

Similar to P-C TVD, the non-linearity of the TVD scheme comes from the $\hat{Q}_{j+1/2}^l$ part of the numerical flux Eq. (36).

The second-order Harten-Yee scheme [29, 28] has the same form as Eq. (35) with

$$\phi^l_{j+1/2} = \frac{1}{2}\psi(a^l_{j+1/2})(g^l_j + g^l_{j+1}) - \psi(a^l_{j+1/2} + \gamma^l_{j+1/2})\alpha^l_{j+1/2}, \tag{37}$$

where

$$\gamma^l_{j+1/2} = \frac{1}{2}\psi(a^l_{j+1/2}) \begin{cases} (g^l_{j+1} - g^l_j)/\alpha^l_{j+1/2} & \alpha^l_{j+1/2} \neq 0 \\ 0 & \alpha^l_{j+1/2} = 0 \end{cases}. \tag{38}$$

Examples of the limiter function g^l_j can be

$$g^l_j = \text{minmod}(\alpha^l_{j-1/2}, \alpha^l_{j+1/2}) \tag{39}$$

or the smooth Eq. (34).

Unlike P-C TVD and the TVD schemes, the second-order MUSCL scheme [28] is fully non-linear. The numerical flux for a MUSCL approach is expressed as

$$\hat{F}_{j+1/2} = \frac{1}{2}(F(U^R_{j+1/2}) + F(U^L_{j+1/2}) - \hat{R}_{j+1/2}\hat{\Phi}_{j+1/2}) \tag{40}$$

with

$$U^R_{j+1/2} = U_{j+1} - \frac{1}{2}\Delta_{j+1} \tag{41}$$

and

$$U^L_{j+1/2} = U_j + \frac{1}{2}\Delta_j. \tag{42}$$

The limiters can be

$$\Delta_j = \text{minmod}(U_{j+1} - U_j, U_j - U_{j-1}) \tag{43}$$

or the smooth Eq. (34). We can see that $U^R_{j+1/2}$ and $U^L_{j+1/2}$ bring non-linearity into every term of the flux Eq. (40).

4 Numerical study

This section performs several numerical examples of flow with non-equilibrium chemistry. We start with a nontrivial steady state to numerically verify whether the considered schemes are well-balanced. Then this steady state is perturbed by small perturbations of different variables. The associated behavior of our schemes will be shown. A shock problem will also be presented in order to test the shock capturing capability of the schemes. In the second part of this section, the same numerical study will be presented for flow in a nozzle.

4.1 Three species model

In all test cases, a simple model for air involving 3 species, O_2, O and N_2 [4] is used. The model has reactions:

$$O_2 + M \rightleftharpoons O + O + M, \tag{44}$$

where M is a catalytic particle (any of the species present).

From Eq. (9), the source term $S(U)$ can be written as

$$S(U) = (2M_1\omega, -M_2\omega, 0, 0, 0), \tag{45}$$

with

$$\omega = \left(k_f(T)\frac{\rho_2}{M_2} - k_b(T)\left(\frac{\rho_1}{M_1}\right)^2 \right)\left(\frac{\rho_1}{M_1} + \frac{\rho_2}{M_2} + \frac{\rho_3}{M_3}\right). \tag{46}$$

The forward reaction rate is

$$k_f = CT^{-2}e^{-E/T}, \tag{47}$$

where $C = 2.9 \times 10^{17}\mathrm{m}^3\mathrm{mole}^{-1}\mathrm{s}^{-1}$ and $E = 59750\mathrm{K}$. The backward reaction rate is

$$k_b = k_f/k_{eq}, \tag{48}$$

with

$$k_{eq} = \exp(b_1 + b_2\log z + b_3 z + b_4 z^2 + b_5 z^3), \quad z = 10000/T, \tag{49}$$

where the constants b_k are found in [4].

We consider the steady state preserving case

$$\begin{cases} (\rho_1)_t = 0 \\ (\rho_2)_t = 0 \\ (\rho_3)_t = 0 \\ v = 0 \\ p = \text{constant} \\ S(U) = 0 \end{cases}. \tag{50}$$

Thus,

$$r = S(U) = \text{constant}, \tag{51}$$

which is of form (21). Note that x and U_x do not appear explicitly in $S(U)$ which is much simpler because all the $t_i'(x) = 1$. Thus any finite-difference operators D_i mentioned in Eq. (16) are absent. Therefore, as described in Sec. 3, linear schemes and WENO-Roe schemes applied to the steady state solution Eq. (50) for the problem Eq. (2) are well-balanced and maintain the original high-order accuracy. WENO-LF, WENO-LLF schemes with suitable modification as described in the previous section are also well-balanced and maintain the original high-order accuracy.

4.1.1 Well-balanced test

The purpose of the first test problem is to numerically verify whether the considered schemes are well-balanced for the special stationary case Eq. (50) with

$$\rho_O = 4 \times 10^{-5}(1 + 0.2\sin(5\pi x))kg/m^3, \qquad p = 10^5 N/m^2, \quad v = 0m/s, \tag{52}$$

with ρ_{O_2} and ρ_{N_2} obtained by the equilibrium state condition. We consider the air which consists of 21% of oxygen and 79% of nitrogen. This can be expressed as

$$\frac{\rho_O}{M_O} + 2\frac{\rho_{O_2}}{M_{O_2}} = \frac{21}{79}\frac{\rho_{N_2}}{M_{N_2}} \tag{53}$$

N	error	error	order	error
	WENO-Roe	WENO-LF		Hybrid WENO-LF
40	5.74E-19	2.31E-09	–	5.56E-17
80	5.26E-19	2.26E-11	6.67	1.87E-17
160	7.05E-19	2.60E-13	6.45	1.20E-16

Table 1: L^1 errors for ρ_O by WENO schemes with N uniform grid points.

N	error	error	error	error	order
minmod limiter	P-C TVD	symmetric TVD	Harten-Yee TVD	MUSCL	
40	9.86E-19	4.74E-21	4.74E-21	3.09E-09	–
80	8.82E-19	4.57E-21	7.96E-21	4.12E-10	3.25
160	9.11E-19	5.08E-21	1.54E-20	2.60E-11	3.98
smooth limiter					
40	4.97E-19	4.40E-21	5.83E-19	4.02E-08	–
80	5.90E-19	4.91E-21	5.60E-19	1.80E-09	4.48
160	7.41E-19	1.45E-19	7.73E-19	3.31E-11	5.76

Table 2: L^1 errors for ρ_O by TVD schemes with minmod/smooth limiter with N uniform grid points, $\delta_1 = 0$.

which holds for the equilibrium state. In the equilibrium state, since there is no reaction, the species also satisfy the source term $S(U) = 0$. This set of steady state solutions is of the form Eq. (50). Eq. (52) is chosen as the initial condition, and the results are obtained by time-accurate time-marching to the steady state.

The error and accuracy at $t = 0.01$ are listed in Tables 1 and 2. It shows that WENO-Roe, P-C TVD and TVD schemes are well-balanced schemes because they produce machine round-off errors. However, WENO-LF and MUSCL schemes are not well-balanced. The hybrid WENO-LF scheme as stated in Sec. 3 is also verified to be well-balanced. We remark that the super convergence of the results for WENO-LF and MUSCL is due to the simple form of the steady state solutions.

Numerically P-C TVD and TVD schemes have been shown to be well-balanced for the steady state solution Eq. (50). Even though the non-linear term $R\Phi$ in the P-C TVD and TVD schemes is not linear, we will explain why this part will not destroy the well-balanced property in these schemes. Since they have similar formulas, we will use the symmetric TVD scheme as the example.

We claim that the function $\Phi = 0$ for the steady state problem Eq. (50). This is due to the fact that v is equal to zero in the steady state solution. Recalling the eigenvalue a in Eq. (10), it is easy to see that only the last two entries a^{n_s+1} and a^{n_s+2} are non-zero. The function ψ is in Eq. (31). If the entropy parameter δ_1 is set to be zero, we will have $\psi(a^l) = |a^l|$. Therefore $\phi^1 \dots \phi^{n_s}$ are always zeros. Note that for any $\delta_1 > 0$, P-C TVD and TVD schemes are not well-balanced.

Next, let us consider the factor $\alpha^l_{j+1/2} - \hat{Q}^l_{j+1/2}$ in Eq. (29) or Eq. (36), where $\alpha^l_{j+1/2}$ is given in Eq. (11).

The resulting equations are obtained directly from the system [7]

$$\alpha^{n_s+k} = (\Delta p \pm a\rho\Delta v)/2a^2 \quad k = 1, 2, \tag{54}$$

where α, v and the frozen speed of sound a are evaluated at the Roe average at $j + 1/2$, and $\Delta p = p_{j+1} - p_j$, etc. Since the pressure p is constant and velocity v is zero in the steady state solution, α^{n_s+1} and α^{n_s+2} are exactly zeros.

Hence, the non-linear term $R\Phi$ is zero and then the P-C TVD and TVD schemes become linear schemes in the steady state solution Eq. (50). By Proposition 1, they are well-balanced schemes towards the steady state solution (50).

4.1.2 Small perturbation

The following test problems will demonstrate the advantages of the well-balanced schemes through the problem of a small perturbation over a stationary state.

The same stationary state solution Eq. (52) is considered. First, a small perturbation $\epsilon = 10^{-10} \times \sin(\pi x)$ (about 0.001%) is added to the density, i.e.,

$$\rho'_O = \rho_O + \epsilon. \tag{55}$$

The other quantities are kept the same. At $t = 0.1$, the differences between the perturbed solutions of density ρ_O and the steady state solutions of density ρ_O are plotted ("Δ" denotes the "difference" in the figures). The reference results are computed by WENO-Roe with 1200 points and are considered to be "exact". To improve the viewing, a factor of 10^{10} is added to all the figures.

The solution of density ρ_O by WENO-Roe is depicted in Fig. 1. The advantage of the well-balanced property of WENO-Roe is clearly demonstrated with only 100 points to resolve such small perturbation. Although the solution indicates two small bumps in the density plot, these bumps disappear when the mesh is refined to 200 points.

Unlike the well-behaved WENO-Roe, the results by WENO-LF, which is not a well-balanced scheme, behave in a very oscillatory fashion using 100 grid points (see Fig. 2 left). This is due to the fact that the well-balanced schemes can resolve the steady state solution exactly, hence they are able to resolve a very small perturbation. However, a scheme that is not well-balanced can only resolve the solution when the mesh is refined enough such that the truncation error of the scheme is much smaller than the perturbation. For example, when the mesh is refined to 300 points for WENO-LF (see Fig. 2 left), the oscillations disappear and the solution is resolved. Fig. 2 right shows the good behavior of the hybrid WENO-LF scheme. It resolves the perturbation perfectly with only 100 points.

Next, the numerical results by P-C TVD, TVD and MUSCL schemes are discussed, respectively. As indicated in Sec. 4.1.1, P-C TVD and TVD schemes are well-balanced schemes for both minmod limiter and smooth limiter. The numerical results of P-C TVD and TVD schemes with smooth limiter show very good agreement with the reference solution (see Figs. 3 right, 4 right and 5 right), whereas the MUSCL scheme, which is not well-balanced, behaves oscillatory (see Fig. 6 right) in the same mesh $N = 300$.

However, note that in Figs. 3 left, 4 left and 5 left, results for P-C TVD and TVD schemes with minmod limiter show some oscillations, and these oscillations do not disappear in the mesh refinement until the mesh is extremely fine. This might be caused by the lack of smoothness of the

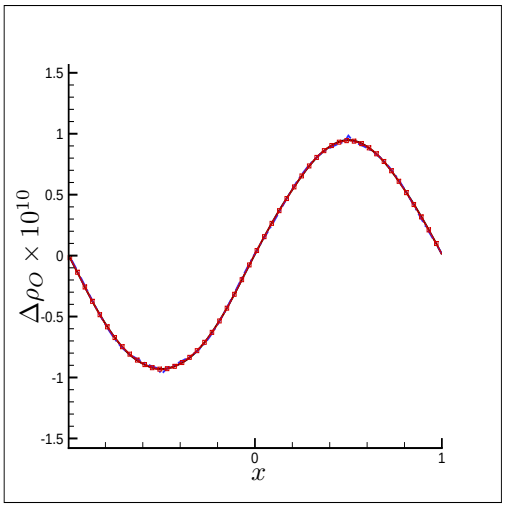

Figure 1: Small perturbation of density results by WENO-Roe: $\epsilon = 10^{-10} \times \sin(\pi x)$. WENO-Roe 100: dash-dot; WENO-Roe 200: dotted with symbols; WENO-Roe 1200: solid.

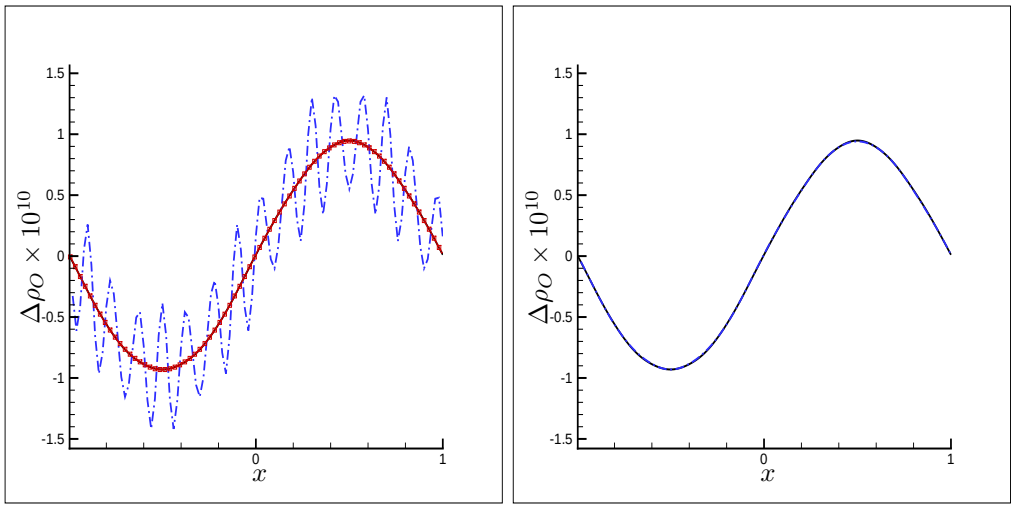

Figure 2: Small perturbation of density results by WENO-LF: $\epsilon = 10^{-10} \times \sin(\pi x)$. Left: WENO-LF (WENO-LF 100: dash-dot; WENO-LF 300: dotted with symbols; WENO-LF 1200: solid); right: hybrid WENO-LF (hybrid WENO-LF 100: dash-dot; WENO-Roe 1200: solid).

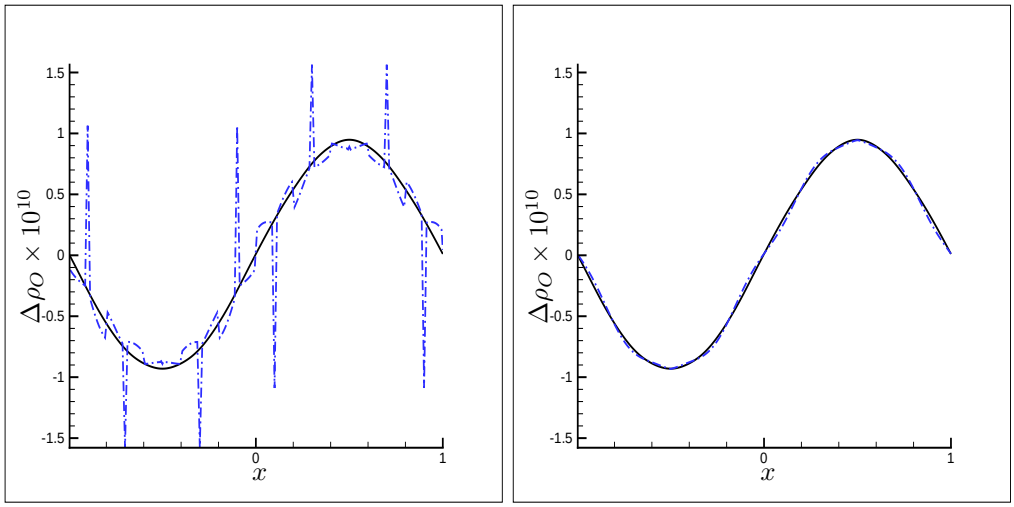

Figure 3: Small perturbation of density results by P-C TVD : $\epsilon = 10^{-10} \times \sin(\pi x)$, $\delta_1 = 0$. Left: with minmod limiter; Right: with smooth limiter (P-C TVD 300: dash-dot; WENO-Roe 1200: solid).

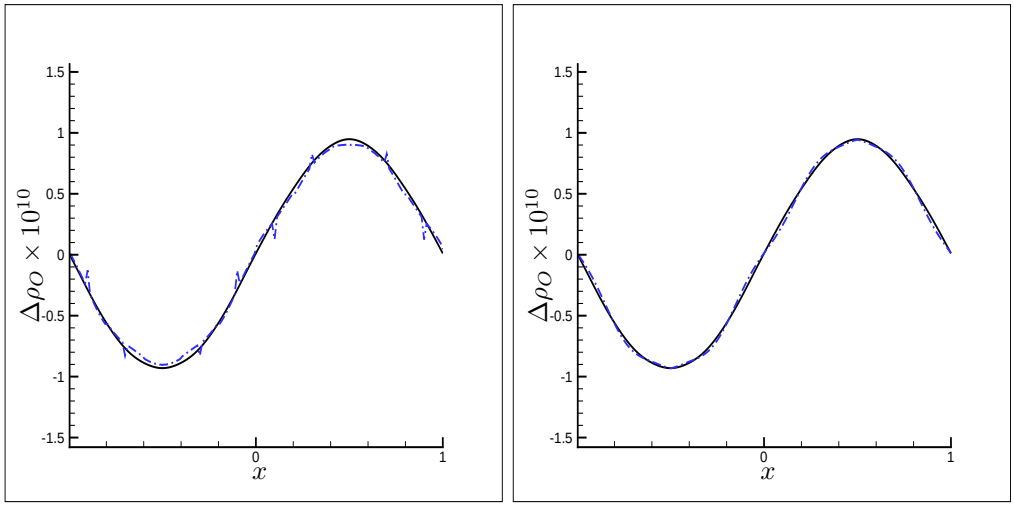

Figure 4: Small perturbation of density results by symmetric TVD: $\epsilon = 10^{-10} \times \sin(\pi x)$, $\delta_1 = 0$. Left: with minmod limiter; Right: with smooth limiter (symmetric TVD 300: dash-dot; WENO-Roe 1200: solid).

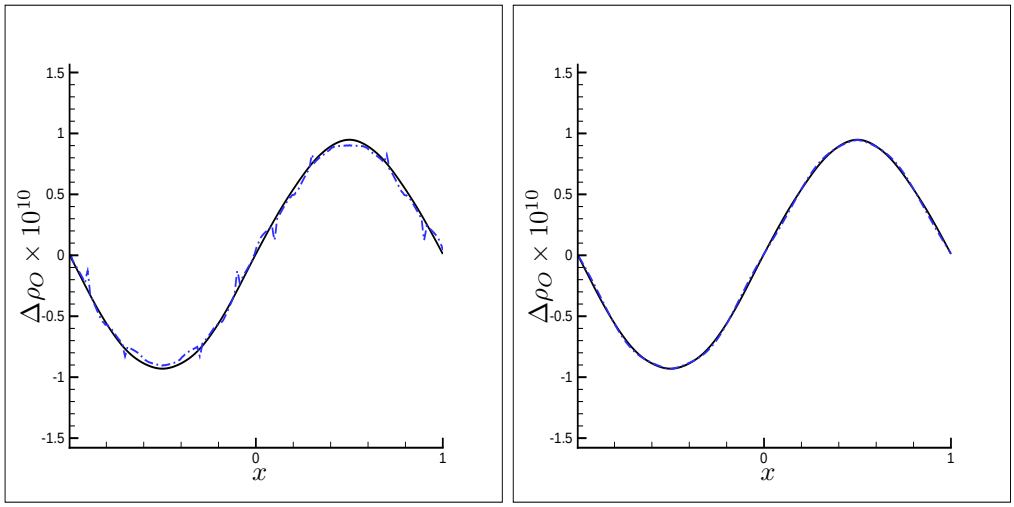

Figure 5: Small perturbation of density results by Harten-Yee TVD: $\epsilon = 10^{-10} \times \sin(\pi x)$, $\delta_1 = 0$. Left: with minmod limiter; Right: with smooth limiter (Harten-Yee 300: dash-dot; WENO-Roe 1200: solid).

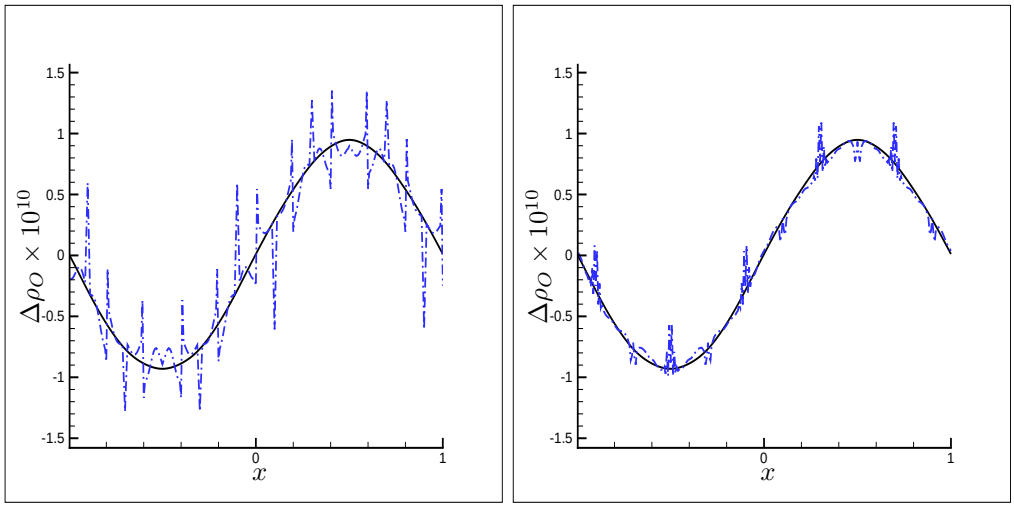

Figure 6: Small perturbation of density results by MUSCL scheme: $\epsilon = 10^{-10} \times \sin(\pi x)$, $\delta_1 = 0$. Left: with minmod limiter; Right: with smooth limiter (MUSCL 300: dash-dot; WENO-Roe 1200: solid).

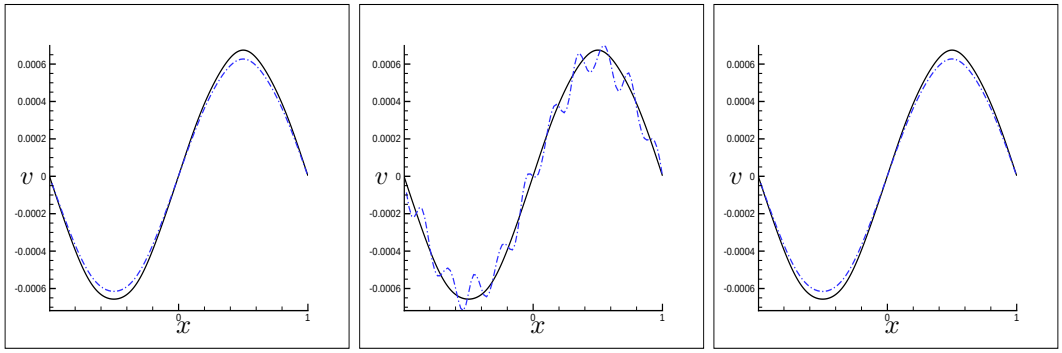

Figure 7: Small perturbation of velocity results. Perturbation of velocity $\epsilon = 10^{-3} \times \sin(\pi x)$. Dash-dot: left: WENO-Roe 100; middle: WENO-LF 100; right: hybrid WENO-LF 100. Solid: WENO-Roe 1200.

minmod limiter, which is continuous but not differentiable. For the sake of this, the smooth limiter will be considered only in the following test problems.

Next our schemes are tested on a perturbation of velocity and a perturbation of energy, i.e.

$$v' = v + \epsilon \tag{56}$$

$$\rho e_0' = \rho e_0 + \epsilon \tag{57}$$

both with $\epsilon = 10^{-3} \times \sin(\pi x)$. Similar to the density case, the difference of the perturbed solutions and the steady state solutions are plotted. But for the velocity case, since the steady state solution is zero, the velocity plots are the perturbed solution. Figs. 7 show the velocity plot under a small perturbation of velocity (56) by WENO-Roe, WENO-LF and hybrid WENO-LF, respectively. The results by P-C TVD, Harten-Yee TVD and MUSCL are shown in Figs. 8. Figs. 9 and 10 show the energy plot under a small perturbation of energy (57) by three WENO schemes and three second order TVD schemes, respectively. Again, the well-balanced schemes WENO-Roe (see Figs. 7 left and 9 left), hybrid WENO-LF (see Figs. 7 right and 9 right), P-C TVD (see Figs. 8 left and 10 left), Harten-Yee TVD (see Figs. 8 middle and Figs. 10 middle) all show very good agreements with the reference solutions even in a coarse mesh. The results by regular WENO-LF (see Figs. 7 middle and 9 middle) have some oscillations in the coarse mesh due to the truncation errors. The results by MUSCL scheme (see Figs. 8 right and 10 right) have much bigger oscillations even on a mesh with 600 grid points. (The non-well balanced WENO-LF behaves better than the MUSCL scheme, due to the high order convergence of the former.)

Through the examples of perturbations of density, velocity and energy, we clearly demonstrate the advantages of using well-balanced schemes in capturing the small perturbation of steady states.

Non-zero entropy fix parameter. Recall in the Sec. 4.1.1, when the entropy fix parameter δ_1 is non-zero, P-C TVD and TVD schemes are not well-balanced schemes for the steady state solution (50). In this section, we will investigate the influence of δ_1 through the small perturbation problems.

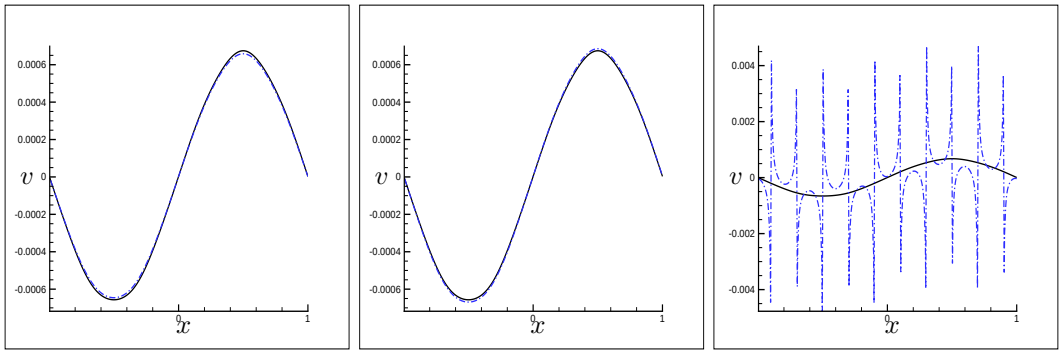

Figure 8: Small perturbation of velocity results. Perturbation of velocity $\epsilon = 10^{-3} \times \sin(\pi x)$, $\delta_1 = 0$. Dash-dot: left: P-C TVD 200; middle: Harten-Yee TVD 300; right: MUSCL scheme 600. Solid: WENO-Roe 1200.

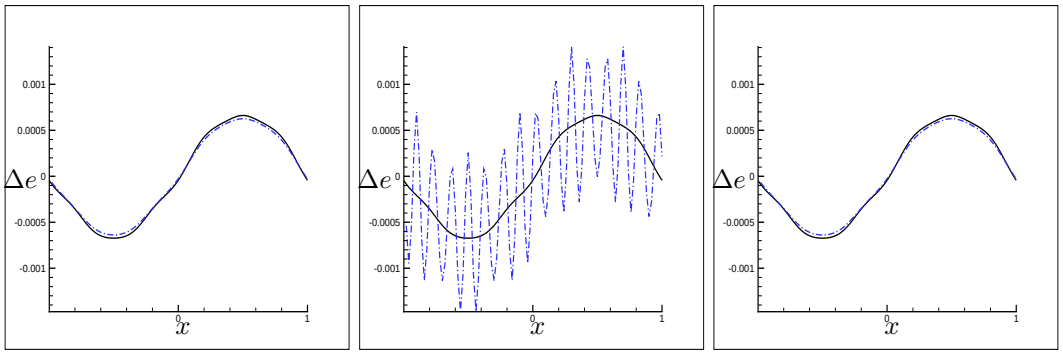

Figure 9: Small perturbation of energy results. Perturbation of energy $\epsilon = 10^{-3} \times \sin(\pi x)$. Dash-dot: left: WENO-Roe 100; middle: WENO-LF 100; right: hybrid WENO-LF 100. Solid: WENO-Roe 1200.

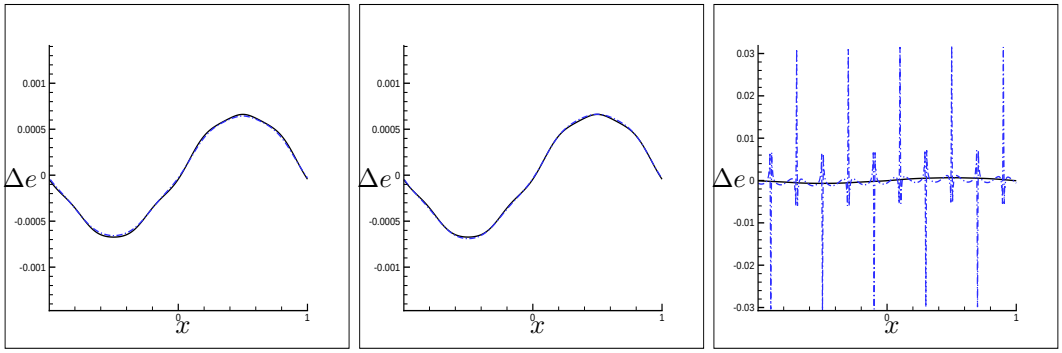

Figure 10: Small perturbation of energy results. Perturbation of energy $\epsilon = 10^{-3} \times \sin(\pi x)$, $\delta_1 = 0$. Dash-dot: left: P-C TVD 200; middle: Harten-Yee TVD 300; right: MUSCL scheme 600. Solid: WENO-Roe 1200.

Figs. 11 show the density plots under a perturbation of density (55) by P-C TVD, Harten-Yee TVD and MUSCL schemes, respectively. Figs. 12 and Figs. 13 show the velocity and energy plots under a perturbation of velocity (56) and energy (57), respectively. Non-zero δ_1 introduces truncation errors into the density equations, which makes P-C TVD and TVD schemes not well-balanced any more. The smaller δ_1 is, the better performance these schemes will have.

In Figs. 11 and 13, the results by P-C TVD and Harten-Yee TVD schemes have smooth fluctuations, which is due to the truncation error by the entropy fix parameter δ_1. MUSCL does not show big difference between zero δ_1 results (see Fig. 8 right) and non-zero δ_1 results (see Fig. 13 right) in the perturbation of energy problem (57), because the truncation error caused by δ_1 is much smaller than the original truncation error. We can see the "better" balanced P-C TVD scheme and Harten-Yee TVD scheme have better performance than the non-well balanced MUSCL scheme.

Unlike the density and the energy cases, in the perturbation of velocity problem (56), the non-zero δ_1 does not have any influence on the velocities (see Figs. 12). This is because the $(n_s + 1)th$ element of $R\Phi$ is always zero as long as the velocity is zero. Thus, the velocity plots for P-C TVD scheme and Harten-Yee TVD scheme remain as good as the zero δ_1 case (see Figs. 8 left and middle).

4.1.3 A shock problem

The third example consists of a shock tube where the high pressure, high temperature on the left half plane and the low pressure, low temperature on the right plane, both contain air, initially in chemical equilibrium. The conditions are:

$$(p_L, T_L) = (1 \times 10^5 N/m^2, 2000K), \quad (p_R, T_R) = (0.6 \times 10^5 N/m^2, 1800K),$$

with zero velocity everywhere and the densities satisfied Eq. (53). Our well-balanced schemes are balanced for the left and right states individually, but not through the transition. The WENO-Roe, hybrid WENO-LF, Harten-Yee and MUSCL schemes are tested. We want to demonstrate that the well (or better) balanced schemes not only behave nicely near the steady state but also can keep good properties far away from steady state, such in capturing shocks. The reference solution is

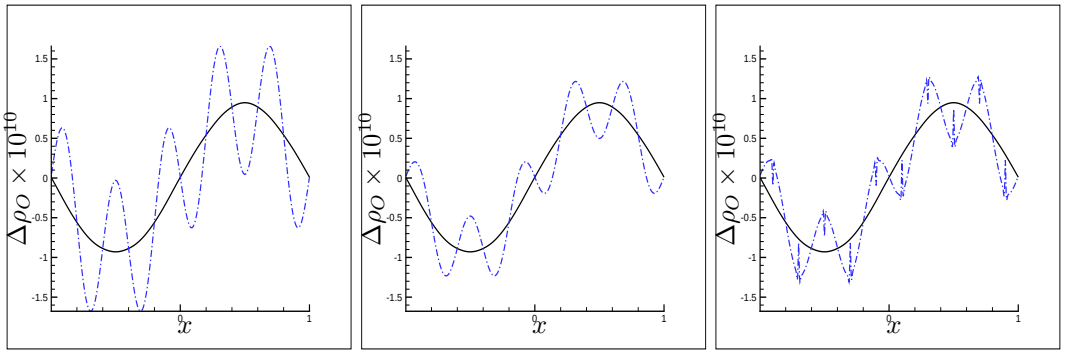

Figure 11: Non-zero entropy fix parameter results of density ρ_O: perturbation of density $\epsilon = 10^{-10} \times \sin(\pi x)$, $\delta_1 = 0.2$. Dash-dot: left: P-C TVD 600; middle: Harten-Yee TVD 600; right: MUSCL scheme 600. Solid: WENO-Roe 1200.

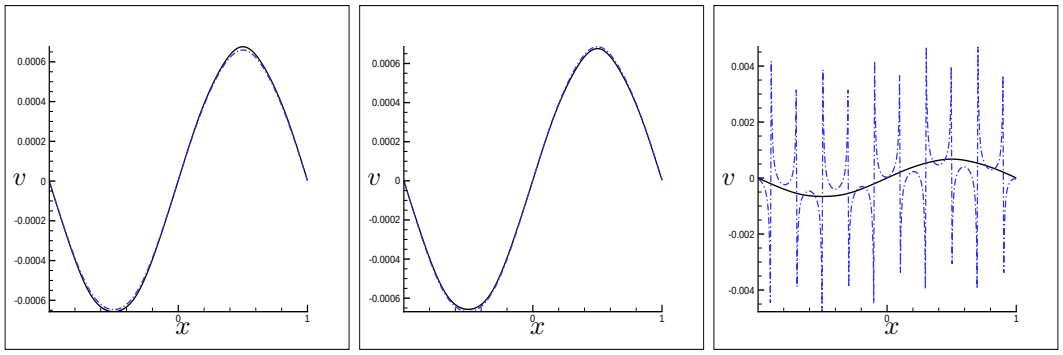

Figure 12: Non-zero entropy fix parameter results of velocity: perturbation of velocity $\epsilon = 10^{-3} \times \sin(\pi x)$, $\delta_1 = 0.2$. Dash-dot: left: P-C TVD 200; middle: Harten-Yee TVD 300; right: MUSCL scheme 600. Solid: WENO-Roe 1200.

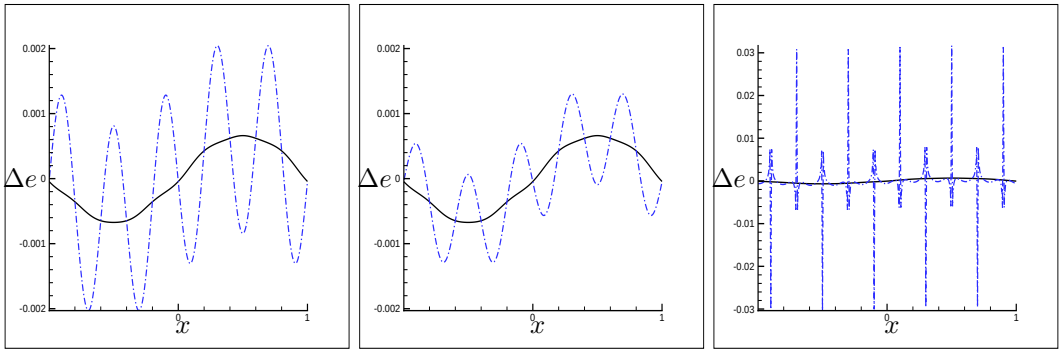

Figure 13: Non-zero entropy fix parameter results of energy: perturbation of energy $\epsilon = 10^{-3} \times \sin(\pi x)$, $\delta_1 = 0.2$. Dash-dot: left: P-C TVD 600; middle: Harten-Yee TVD 600; right: MUSCL scheme 600. Solid: WENO-Roe 1200.

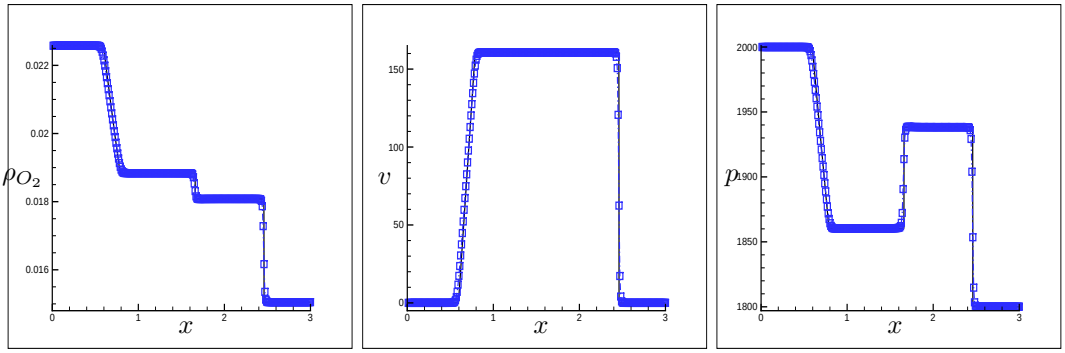

Figure 14: Riemann problem: left: density; middle: velocity; right: pressure (WENO-Roe 300: dash line with symbols; WENO-LF 12000: solid).

taken to be regular WENO-LF with 12000 points. The results by WENO-Roe, hybrid WENO-LF, Harten-Yee and MUSCL schemes at $t = 0.001$ are shown in Figs. 14, Figs. 15, Figs. 17 and Figs. 18, respectively. For each scheme, the figures of density, velocity and pressure are plotted from left to right. The hybrid WENO-LF gives well resolved, non-oscillatory solutions using 300 uniform cells.

4.2 Nozzle flow

In this section, the quasi-one-dimensional non-equilibrium nozzle flow with the reaction terms (see the equilibrium nozzle flow [3]) is considered. The governing equations for the non-equilibrium flow with 3 species ($\rho_1 = O$, $\rho_2 = O_2$, $\rho_3 = N_2$) through a duct of varying cross-section can be written

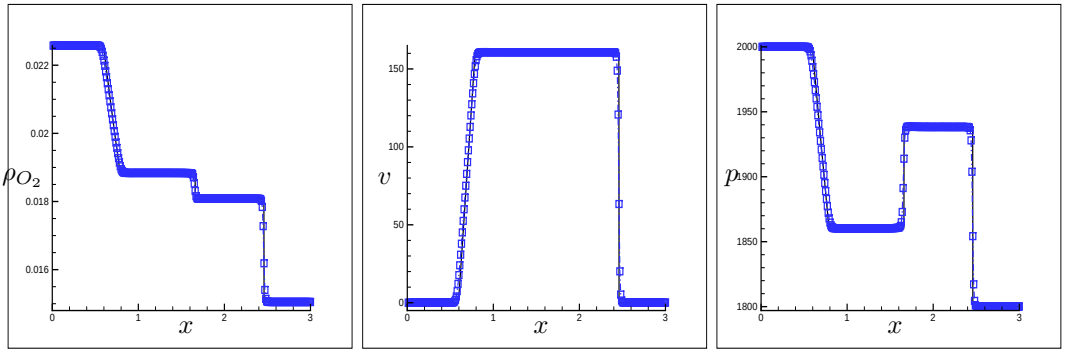

Figure 15: Riemann problem: left: density; middle: velocity; right: pressure (hybrid WENO-LF 300: dash line with symbols; WENO-LF 12000: solid).

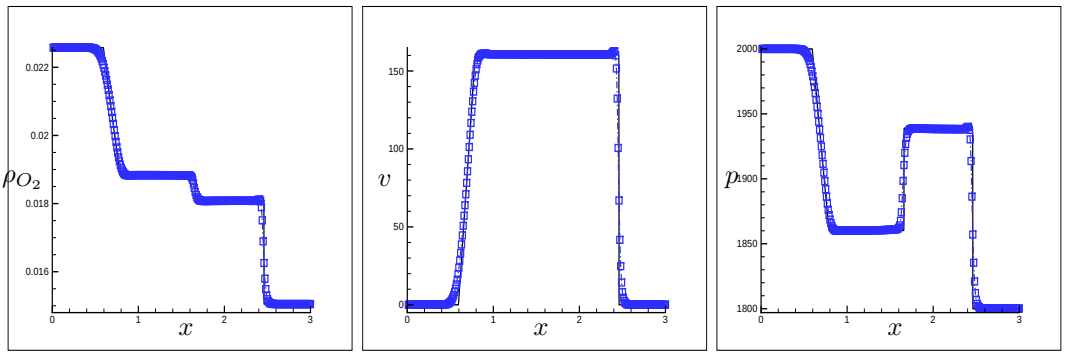

Figure 16: Riemann problem: left: density; middle: velocity; right: pressure (P-C TVD 300: dash line with symbols; WENO-LF 12000: solid).

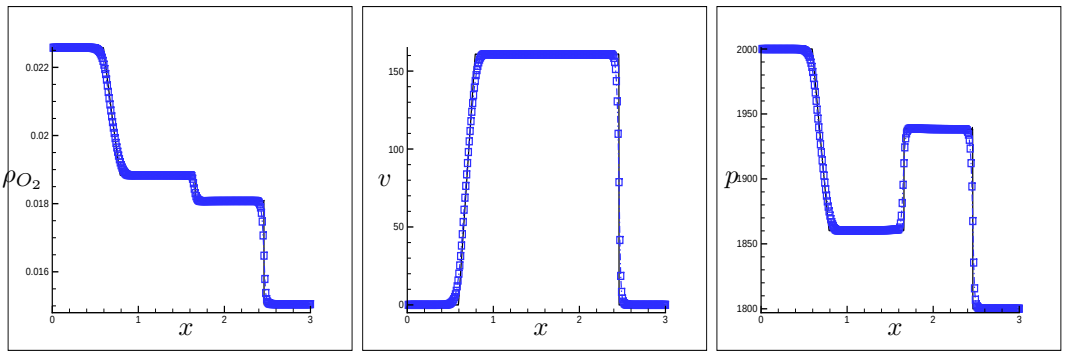

Figure 17: Riemann problem: left: density; middle: velocity; right: pressure (Harten-Yee TVD 300: dash line with symbols; WENO-LF 12000: solid).

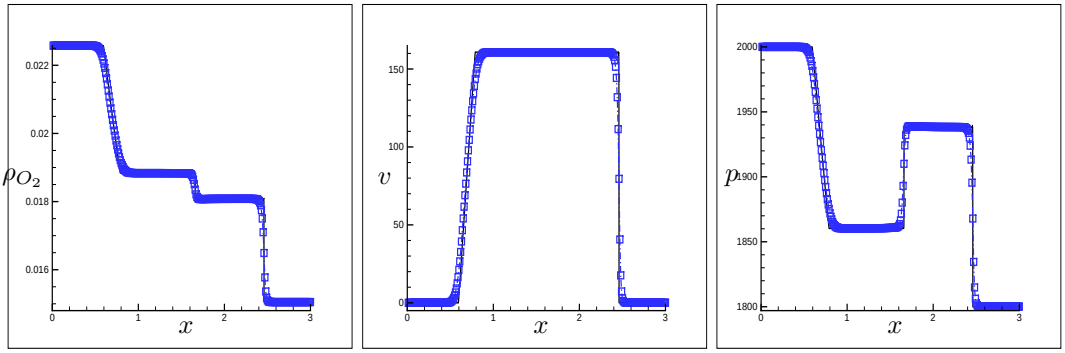

Figure 18: Riemann problem: left: density; middle: velocity; right: pressure (MUSCL scheme 300: dash line with symbols; WENO-LF 12000: solid).

in conservation form as:

$$\begin{aligned}
&(\rho_i A)_t + (\rho_i v A)_x = s^i, \quad i = 1, \ldots, 3, \\
&(\rho v A)_t + \big((\rho v^2 + p)A\big)_x = pA'(x), \\
&(\rho e_0 A)_t + ((\rho e_0 + p)vA)_x = 0,
\end{aligned} \tag{58}$$

where $A = A(x)$ denotes the area of the cross section and s^i is given by Eq. (45).

4.2.1 Well-balanced test

First the well-balanced properties of our schemes are tested for the same steady state (52), for which the cross section area and the initial conditions are taken as

$$A(x) = 1 + \sin(\pi x), \quad 0 \le x \le 2, \tag{59}$$

$$v(x,0) = 0m/s, \quad p(x,0) = 10^5 N/m^2, \quad T(x,0) = 2000K, \tag{60}$$

with periodic boundary conditions. The densities of each species are obtained by the equilibrium state condition $S(U) = 0$ and Eq. (53).

The balanced WENO-LF scheme (20) is considered in this section. We take

$$\begin{cases} r_i(U,x) = \rho_i \quad i = 1, \ldots, 3 \\ r_4(U,x) = v \\ r_5(U,x) = p \end{cases}, \tag{61}$$

which are of form (21) in the steady state (60).

Note that an extra source term $pA'(x)$ in addition to the chemical reaction terms is appeared in Eq. (58). As stated in Sec. 3, this term needs special treatment in order to get the well-balanced WENO schemes. First, $pA'(x)$ is written in form of (15) with $s(r(u,x)) = p$ and $t(x) = A(x)$. Then, it is approximated by the same operator of the flux, i.e., Eq. (18).

Table 3 lists the errors and accuracies of regular WENO schemes and balanced WENO-LF scheme at $t = 0.01$. As shown in Table 3, none of the regular WENO schemes are well-balanced if just pointwise evaluation is used to the source term. (It is different from the problem in Sec.

N	error	order	error	order	error
	WENO-Roe		WENO-LF		Balanced WENO-LF
40	2.21E-07	–	4.08E-07	–	2.28E-16
80	6.95E-09	4.99	1.31E-08	4.96	3.59E-16
160	2.17E-10	5.00	4.10E-10	4.99	6.89E-16
320	6.75E-12	5.01	1.28E-11	5.00	9.14E-16

Table 3: L^1 errors of ρ_{O_2} for nozzle flow by WENO schemes with N uniform grid points.

N	error	order	error	order
	Harten-Yee		MUSCL	
40	4.13E-05	–	1.50E-05	–
80	9.75E-06	2.08	5.59E-06	1.43
160	3.17E-06	1.62	1.56E-06	1.84
320	9.73E-07	1.70	4.25E-07	1.87
640	2.19E-07	2.16	1.12E-07	1.94

Table 4: L^1 errors of ρ_{O_2} for nozzle flow by TVD schemes with N uniform grid points.

4.1.1, when there is no spatial derivative involved in the source term, the WENO-Roe scheme is well-balanced.) We see a clean fifth order accuracy for the regular WENO schemes. The balanced WENO-LF scheme (20) with special treatment to the source term (18) gives round-off errors which maintains the steady state solution (60) exactly.

Table 4 lists the errors and accuracies of Harten-Yee TVD scheme and MUSCL TVD scheme. Harten-Yee TVD scheme appears to be not well-balanced in this case. Recall the analysis in Sec. 4.1.1,

$$\alpha^{ns+k} = (\Delta(A(x)p) \pm aA(x)\rho\Delta v)/2a^2 \quad k = 1, 2 \tag{62}$$

for the nozzle flow problem Eq. (58), thus α^{ns+1} and α^{ns+2} are no longer zeros. Both Harten-Yee TVD scheme and MUSCL TVD scheme show a second order accuracy for the well-balanced test.

4.2.2 Small perturbation

The following test case is chosen to demonstrate the capability of the proposed scheme for computations on the perturbation of the steady-state solution (60), which cannot be captured well by a non-well balanced scheme.

A perturbation of density ρ_{O_2} is considered, i.e.,

$$\rho'_{O_2} = \rho_{O_2} + \epsilon \tag{63}$$

with $\epsilon = 10^{-5} \times \sin(\pi x)$ (about 0.1% of the quantity). The plot of density ρ_{O_2} at the time $t = 0.05$ is shown in Fig. 19. The regular WENO-LF scheme with $N = 1200$ is used as a reference solution. The balanced WENO-LF can capture the perturbation very well in a mesh size 60. However, neither of Harten-Yee or MUSCL scheme can do that in a coarse mesh. Similarly, we perturb the velocity

$$v' = v + \epsilon \tag{64}$$

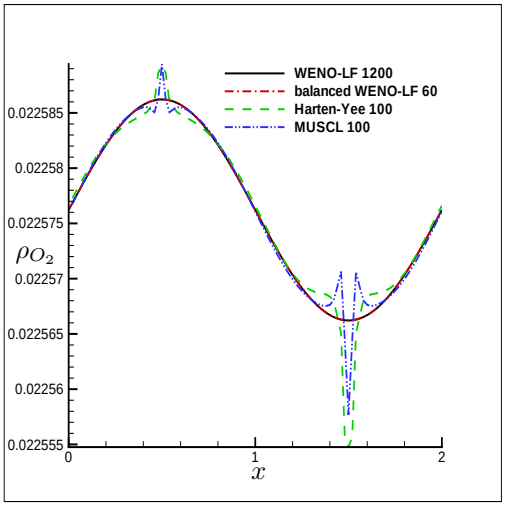

Figure 19: Small density perturbation of the nozzle flow.

with $\epsilon = 0.5 \times \sin(\pi x)$ and the pressure

$$p' = p + \epsilon \tag{65}$$

with $\epsilon = 10 \times \sin(\pi x)$ separately. The well-balanced WENO-LF scheme again presents good resolution of small perturbations in the plots of velocity (see Fig. 20) and pressure (see Fig. 21). However, the non-well balanced schemes show spurious oscillations and need more points to resolve the solution.

4.2.3 A shock problem

Proposed by Anderson in [1], it is concerned with a convergent-divergent nozzle flow with a parabolic area distribution, which is given by

$$A(x) = 1 + 2.2(x - 1.5)^2, \quad 0 \leq x \leq 3. \tag{66}$$

The initial conditions are taken as the equilibrium state of

$$v(x, 0) = 0m/s, \quad p(x, 0) = 10^5 N/m^2, \quad T(x, 0) = 2000K.$$

The boundary conditions are taken as one bar of pressure at the left, 0.6784 bar of pressure at the right, and 2000 K of temperature at both ends. The boundary conditions for the density of each species are obtained from the equilibrium conditions at the boundaries. A shock is established inside the pipe. The computation is performed using $N = 200$ points at $t = 0.1$. The pressure p and velocity v are plotted.

The results by balanced WENO-LF scheme are shown in Figs. 22. The numerical resolution is very good without oscillations, verifying the essentially non-oscillatory property of the balanced WENO-LF scheme. The results by Harten-Yee TVD and MUSCL are also presented in Figs. 23 and 24, respectively.

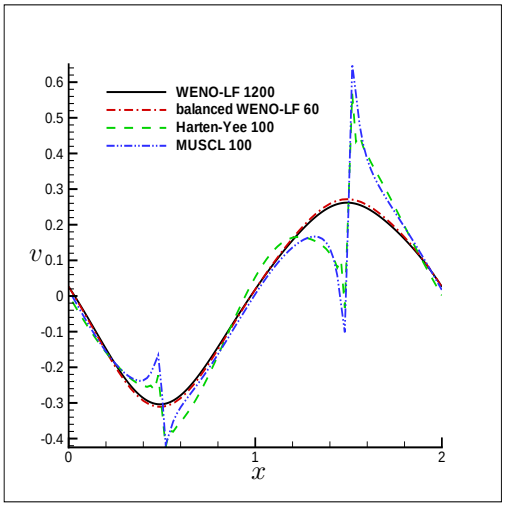

Figure 20: Small velocity perturbation of the nozzle flow.

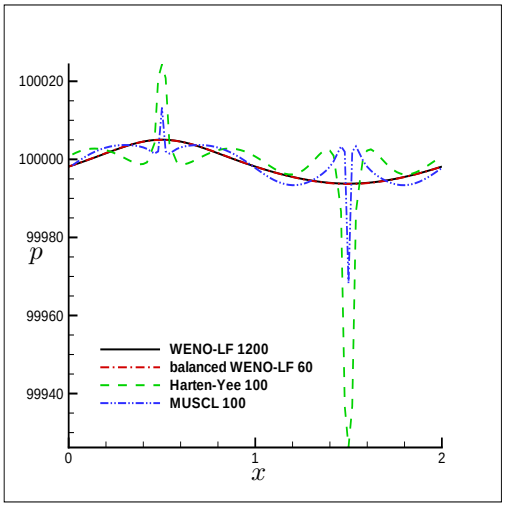

Figure 21: Small pressure perturbation of the nozzle flow.

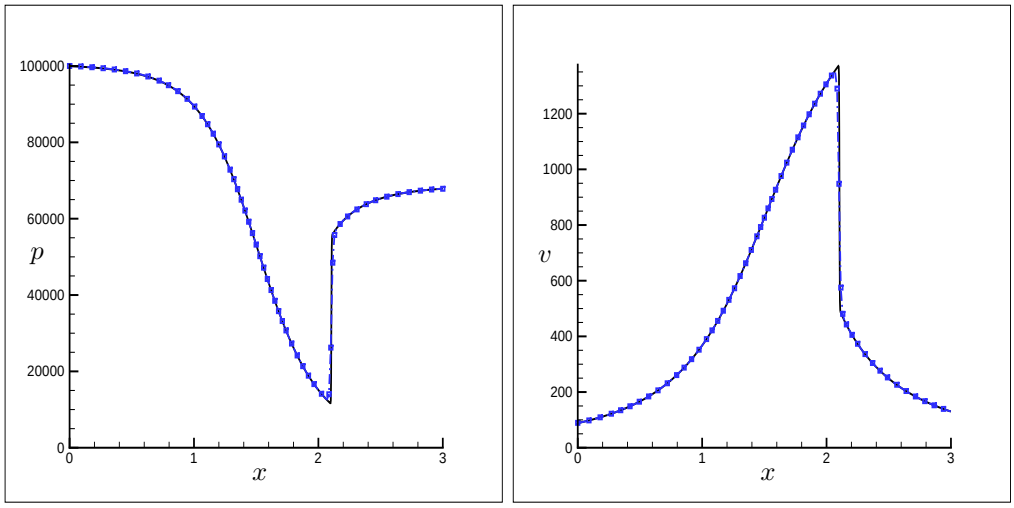

Figure 22: Nozzle flow: (a) left: pressure; (b) right: velocity (balanced WENO-LF 200: dash line with symbols; WENO-LF 1200: solid).

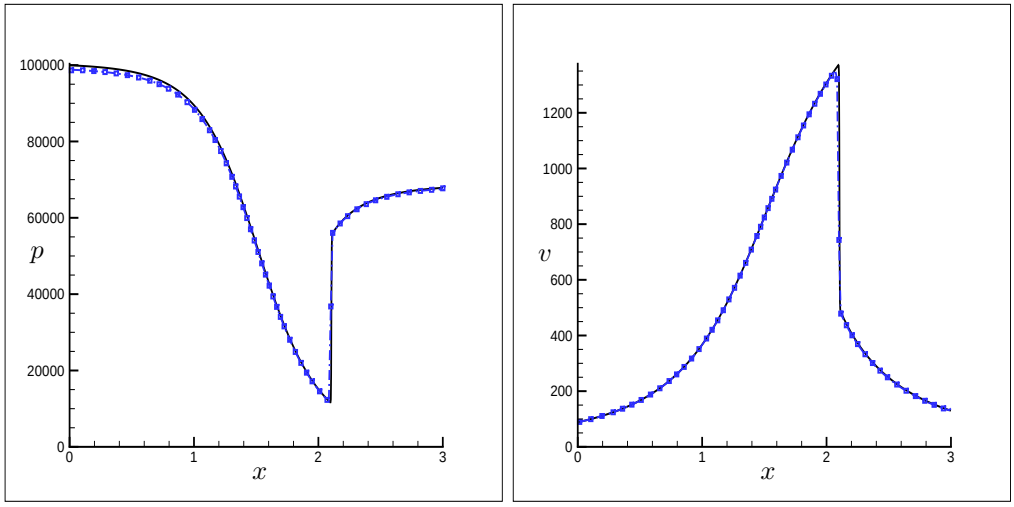

Figure 23: Nozzle flow: (a) left: pressure; (b) right: velocity (Harten-Yee scheme 200: dash line with symbols; WENO-LF 1200: solid).

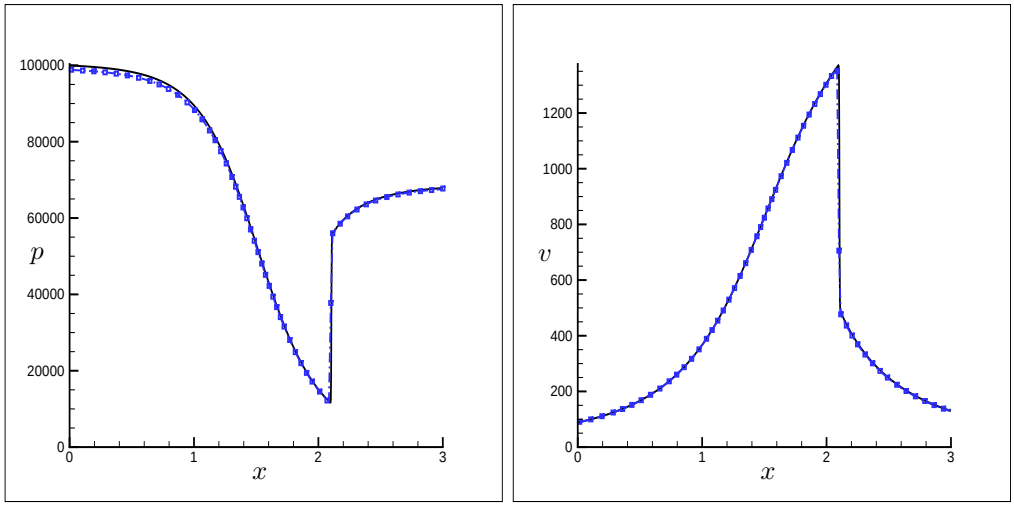

Figure 24: Nozzle flow: (a) left: pressure; (b) right: velocity (MUSCL scheme 200: dash line with symbols; WENO-LF 1200: solid).

5 Concluding remarks

The current results serve as a preliminary study on well-balanced schemes for non-equilibrium flow with source terms. The well-balanced WENO schemes are constructed for the non-equilibrium flow. Numerical examples are given to demonstrate the well-balanced property, accuracy, good capturing of the small perturbation to the steady state solutions, and the non-oscillatory shock resolution of the proposed numerical method. Future research will apply the same approach to analyze the well-balanced properties for the model with larger number of species, and for multi-dimensional flows. A more general type of steady state problem with non-zero velocity will also be considered. In this case, the source terms are balanced by the flux gradients. Special attention will be paid to general reactive flows for which perturbation from equilibrium states could be small in some parts of the domain and large in other parts.

A Appendix: Additive Runge-Kutta Scheme

The implicit time method we are interested in is Additive Runge-Kutta Scheme (ARK) introduced by Kennedy and Carpenter [12].

Rewrite Eq. (2) as

$$\begin{cases} U_t = F_N(t, U(t)) + F_S(t, U(t)), \\ U(0) = U_0, \end{cases} \tag{67}$$

where F_N denotes the non-stiff term and F_S denotes the stiff term.

Table 5: The coefficients for ARK3.

	$j=0$	$j=1$	$j=2$	$j=3$
$a_{ij}^{[N]}$				
$i=1$	$\frac{1767732205903}{2027836641118}$			
$i=2$	$\frac{5535828885825}{10492691773637}$	$\frac{788022342437}{10882634858940}$		
$i=3$	$\frac{6485989280629}{16251701735622}$	$-\frac{4246266847089}{9704473918619}$	$\frac{10755448449292}{10357097424841}$	
$a_{ij}^{[S]}$				
$i=1$	$\frac{1767732205903}{4055673282236}$	$\frac{1767732205903}{4055673282236}$		
$i=2$	$\frac{2746238789719}{10658868560708}$	$-\frac{640167445237}{6845629431997}$	$\frac{1767732205903}{4055673282236}$	
$i=3$	$\frac{1471266399579}{7840856788654}$	$-\frac{4482444167858}{7529755066697}$	$\frac{11266239266428}{11593286722821}$	$\frac{1767732205903}{4055673282236}$
$b_j^{[N]}$	$\frac{1471266399579}{7840856788654}$	$-\frac{4482444167858}{7529755066697}$	$\frac{11266239266428}{11593286722821}$	$\frac{1767732205903}{4055673282236}$
$b_j^{[S]}$	$\frac{1471266399579}{7840856788654}$	$-\frac{4482444167858}{7529755066697}$	$\frac{11266239266428}{11593286722821}$	$\frac{1767732205903}{4055673282236}$
c_j	0	$\frac{1767732205903}{2027836641118}$	0.6	1

The ARK scheme to Eq. (67) has the following form

$$U^{(i)} = U^n + \Delta t \sum_{j=0}^{i-1} a_{ij}^{[N]} F_N(t^n + c_j \Delta t, U^{(j)}) + \Delta t \sum_{j=0}^{i} a_{ij}^{[S]} F_S(t^n + c_j \Delta t, U^{(j)}), \tag{68}$$

$$U^{n+1} = U^n + \Delta t \sum_{j=0}^{s} b_j^{[N]} F_N(t^n + c_j \Delta t, U^{(j)}) + \Delta t \sum_{j=0}^{s} b_j^{[S]} F_S(t^n + c_j \Delta t, U^{(j)}), \tag{69}$$

where $U^{(0)} = U^n$ and $U^{(i)}$ approximates $U(t^n + c_i \Delta t), \quad i = 1, \ldots, s$. The non-stiff and stiff terms are integrated by their own $(s+1)$-stage Runge-Kutta methods respectively.

The coefficients $a_{ij}^{[N]}$, $a_{ij}^{[S]}$, $b_j^{[N]}$, $b_j^{[S]}$, c_j are constrained by order of accuracy and stability considerations. A third-order ARK method are considered in the computation.

The coefficients for the 3rd order ARK method (ARK3) we use are list in Table 5. For more details, we refer the readers to [12].

For the second-order schemes such as Harten-Yee and MUSCL, we use a simple second-order Implicit-explicit Runge-Kutta scheme (IE2) for the time discretization, which has the form

$$\begin{aligned} U^{(1)} &= U^n + \Delta t F_N(t^n, U^n) + a \Delta t F_S(t^n, U^n), & (70)\\ U^{n+1} &= (U^{(1)} + U^n)/2 + \Delta t F_N(t^{n+1}, U^{(1)})/2 & (71)\\ &\quad + b \Delta t F_S(t^n, U^{(1)}) + c \Delta t F_S(t^{n+1}, U^{n+1}), \end{aligned}$$

where the coefficients are

$$a = 1 \quad b = 0 \quad c = 1/2. \tag{72}$$

Remark 1. *In the steady state or close to steady state problems, the source term is close to zero and thus not stiff. Both an explicit and an implicit time methods can be used. However, in the state away steady state, such as the shock problem in 4.1.3, using an implicit time method allows a large*

Table 6: cfl numbers based on numerical test

N	WENO		2nd order TVD schemes			
	RK3	ARK3	RK2	IE2	RK3	ARK3
10	0.1	1.0	0.09	0.7	0.1	1.0
20	0.2	1.0	0.1	0.7	0.2	1.0
40	0.4	1.1	0.3	0.7	0.4	1.1
80	0.8	1.2	0.7	0.7	0.8	1.2
100	0.9	1.3	0.7	0.7	1.0	1.3

cfl number and thus saves computational cost. In Table 6, we list the maximum cfl numbers allowed for WENO scheme and second order TVD schemes (Harten-Yee and MUSCL) with different time discretizations mentioned in Appendix A. Implicit methods show big advantage of saving computational cost especially in coarse mesh. When the mesh is refined, the source term becomes less stiff.

Acknowledgments

The authors acknowledge the support of the DOE/SciDAC grant xxxxx. The work by Bjorn Sjögreen is performed under the auspices of the U.S. Department of Energy by Lawrence Livermore National Laboratory under Contract DE-AC52-07NA27344.

References

[1] Anderson, J. D. 1995 Computational Fluids Dynamics, *McGraw-Hill, New York.*

[2] Engquist, B. & Sjögreen, B. 1991 Robust difference approximation for stiff inviscid detonation waves, *Report CAM 91-05, Dept. of Math., UCLA.*

[3] Gascón, Ll., & Corberán, J. M. 2001 Construction of second-order TVD schemes for nonhomogeneous hyperbolic conservation laws, *J. Comp. Phys.* **172**, 261–297.

[4] Gnoffo, P. A., Gupta, R. N. & Shinn, J. L. 1989 Conservation equations and physical models for hypersonic air flows in thermal and chemical nonequilibrium, *NASA Technical Paper* **2867**, 1–58.

[5] Greenberg, J. M., & LeRoux, A. Y. 1996 A well-balanced scheme for the numerical processing of source terms in hyperbolic equations, *SIAM J. Numer. Anal.* **33**, 1–16.

[6] Griffiths, D. F., Stuart, A. M., & Yee, H. C. 1992 Numerical wave propagation in hyperbolic problems with nonlinear source terms, *SIAM J. Numer. Anal.* **29**, 1244–1260.

[7] Grossman, B. & Cinnella, P. 1990 Flux-split algorithms for flows with non-equilibrium chemistry and vibrational relaxation, *J. Comp. Phys.* **88**, 131–168.

[8] Harten, A., Lax, P. D., & Van Leer, B. 1983 On upstream differencing and Godunov-type schemes for hyperbolic conservation laws, *SIAM Review* **25**, 35–61.

[9] Hubbard, M. E., & Garcia-Navarro, P. 2000 Flux difference splitting and the balancing of source terms and flux gradients, *J. Comp. Phys.* **165**, 89–125.

[10] Jiang, G. & Shu, C.-W. 1996 Efficient implementation of weighted ENO schemes, *J. Comp. Phys.* **126**, 202–228.

[11] Jin, S. 2001 A steady-state capturing method for hyperbolic systems with geometrical source terms, *Mathematical Modelling and Numerical Analysis (M^2AN)* **35**, 631–645.

[12] Kennedy, C. A. & Carpenter, M. H. 2003 Additive Runge-Kutta schemes for convection-diffusion-reaction equations, *Appl. Numer. Math.* **44**, 139–181.

[13] Kurganov, A., & Levy, D. 2002 Central-upwind schemes for the Saint-Venant system, *Mathematical Modelling and Numerical Analysis (M^2AN)* **36**, 397–425.

[14] Lafon, A. & Yee, H. C. 1996 Dynamical approach study of spurious steady-state numerical solutions for non-linear differential equations, Part III: The effects of non-linear source terms in reaction-convection equations, *Comp. Fluid Dyn.* **6**, 1–36.

[15] Lafon, A. & Yee, H. C. 1996 Dynamical approach study of spurious steady-state numerical solutions for non-linear differential equations, Part IV: Stability vs. numerical treatment of non-linear source terms, *Comp. Fluid Dyn.* **6**, 89–123.

[16] LeVeque, R. J. 1998 Balancing source terms and flux gradients in high-resolution Godunov methods: the quasi-steady wave-propagation algorithm, *J. Comp. Phys.* **146**, 346–365.

[17] LeVeque, R. J. & Yee, H. C. 1990 A study of numerical methods for hyperbolic conservation laws with stiff source terms, *J. Comp. Phys.* **86**, 187–210.

[18] Noelle, S. Xing, Y. & Shu, C.-W. 2007 High order well-balanced finite volume WENO schemes for shallow water equation with moving water, *J. Comp. Phys.* **226**, 29–58.

[19] Rebollo, T. C., Delgado, A. D., & Nieto, E. D. F. 2003 A family of stable numerical solvers for the shallow water equations with source terms, *Computer Methods in Applied Mechanics and Engineering* **192**, 203–225.

[20] Roe, P. L. 1981 Approximate Riemann solvers, parameter vectors, and difference schemes, *J. Comp. Phys.* **43**, 357–372.

[21] Russo, G. 2000 Central schemes for balance laws, *in: Proceedings of the VIII International Conference on Nonlinear Hyperbolic Problems, Magdeburg.*

[22] Shu, C.-W. 1998 Essentially non-oscillatory and weighted essentially non-oscillatory schemes for hyperbolic conservation laws, *in: B. Cockburn, C. Johnson, C.-W. Shu, E. Tadmor (Ed.: A. Quarteroni) Advanced Numerical Approximation of Nonlinear Hyperbolic Equations, Lecture Notes in Mathematics, vol. 1697, Springer,* 325–432.

[23] Shu, C.-W. & Osher, S. 1988 Efficient implementation of essentially non-oscillatory shock-capturing schemes, *J. Comp. Phys.* **77**, 439–471.

[24] Xing, Y. & Shu, C.-W. 2005 High order finite difference WENO schemes with the exact conservation property for the shallow water equations, *J. Comp. Phys.* **208**, 206–227.

[25] Xing, Y. & Shu, C.-W. 2006 High order well-balanced finite difference WENO schemes for a class of hyperbolic systems with source terms, *J. Sci. Comp.* **27**, 477–494.

[26] Xu, K. 2002 A well-balanced gas-kinetic scheme for the shallow-water equations with source terms, *J. Comp. Phys.* **178**, 533–562.

[27] Yee, H. C. 1987 Construction of explicit and implicit symmetric TVD schemes and their applications, *J. Comp. Phys.* **68**, 151–179.

[28] Yee, H. C. 1989 A class of high-resolution explicit and implicit shock-capturing methods, *VKI lecture series 1989-04, March 6-10, 1989; NASA TM-101088, Feb. 1989.*

[29] Yee, H. C. & Harten, A. 1987 Implicit TVD schemes for hyperbolic conservation laws in curvilinear coordinates, *AIAA Journal* **25**, 266–274.

[30] Yee, H. C. & Shinn, J. L. 1989 Semi-implicit and fully implicit shock-capturing methods for nonequilibrium flows, *AIAA Journal* **225**, 910–934.

[31] Yee, H. C. & Sjögreen, B. 2007 Development of low dissipative high order filter schemes for multiscale Navier-Stokes/MHD systems, *J. Comp. Phys.* **68**, 151–179.

[32] Yee, H. C., Sweby, P. K. & Griffiths, D. F. 1991 Dynamical approach study of spurious steady-state numerical solutions for non-linear differential equations, Part I: The dynamics of time discretizations and its implications for algorithm development in computational fluid dynamics, *J. Comp. Phys.* **97**, 249–310.

[33] Zhou, J. G., Causon, D. M., Mingham, C. G. & Ingram, D. M. 2001 The surface gradient method for the treatment of source terms in the shallow-water equations, *J. Comp. Phys.* **168**, 1–25.